Pergamon

PII: S0301-9322(96)00081-X

Int. J. Multiphase Flow Vol. 23, No. 3, pp. 523–543, 1997

Printed in Great Britain
0301-9322/97 $17.00 + 0.00

ANALYTICAL SOLUTION FOR LAMINAR TWO-PHASE FLOW IN A FULLY ECCENTRIC CORE–ANNULAR CONFIGURATION

J. ROVINSKY, N. BRAUNER and D. MOALEM MARON
Department of Fluid Mechanics, School of Engineering, Tel-Aviv University, Israel

(Received 29 April 1996; in revised form 17 October 1996)

Abstract—Fully eccentric and concentric core annular flows represent two extremes which are of practical interest with regard to the performance of core flows. The fully eccentric configuration, which is obviously the problematic one, has been tackled herein by introducing a unipolar coordinate system, since the bipolar coordinate system fails to describe the flow field for this extreme.

The analytical solution obtained yields the velocity profiles, wall and interfacial shear stresses and the resulting insitu holdup and pressure drop. The determination of the flow characteristics for fully eccentric flows is important as a bound to evaluate the effect of the core eccentricity in annular flows and as a complementary information to previous solutions of stratified flows with curved interface.

Key Words: cone, annular, eccentricity, stratified, curved interface

1. INTRODUCTION

Fully eccentric core–annular flows can be realized as an extreme configuration of either stratified flow patterns or annular flow patterns (figure 1). The stratified and annular flows are considered basic flow configurations which are realized in a variety of two-fluid systems. Analytical models for annular or stratified configuration are oftern the starting points for analyzing transitions to other possible flow patterns. As such, the stratified and annular flow patterns attain a continuous intensified interest from both the practical and theoretical points of view. However, analytical solutions for both stratified and annular flows exhibit difficulties when converging to the configuration of fully eccentric core flow. Therefore, the fully eccentric configuration ought to be tackled directly. A brief review of relevant existing solutions for the various flow configurations encountered follows.

Stratified layers may exhibit a plane or a curved interface. A plane interface is characteristic to gravity dominated systems as in the case in large scale air-water systems under earth gravitation. However, in two-fluid systems of small density differential (e.g. liquid–liquid, vapor–liquid near the critical point), reduced gravity systems or capillary systems, surface phenomena become important, and the interface demonstrates a curved shape (convex or concave). The controlling non-dimensional parameters are the fluids/wall wettability angle, α and the Eötvös number. The latter represents the ratio between surface and gravity forces (Brauner 1990; Rovinsky *et al.* 1995):

$$\epsilon_v = \frac{2\sigma_{12}}{(\rho_2 - \rho_1)gR^2} \qquad [1]$$

where ρ_1, ρ_2 are the fluids densities, σ_{12} is their surface tension and R is the tube radius.

The characteristic interface curvature has been predicted by employing energy considerations (Brauner *et al.* 1996b). Stratification with plane interface is realized in systems of $\epsilon_v \to 0$, while for $\epsilon_v \gg 1$, the stratified configuration approaches a fully eccentric core-annular configuration (figure 1c, g). Figure 1(g) corresponds to ideal wettability of the upper fluid, where the upper fluid spreads over the wall to form the annuli and the lower heavier phase forms a fully eccentric core at the tube bottom. The other extreme, shown in figure 1(c), corresponds to $\epsilon_v \gg 1$ and ideal wettability of the lower heavier phase (Brauner *et al.* 1995, 1996b). Stratified configurations with curved

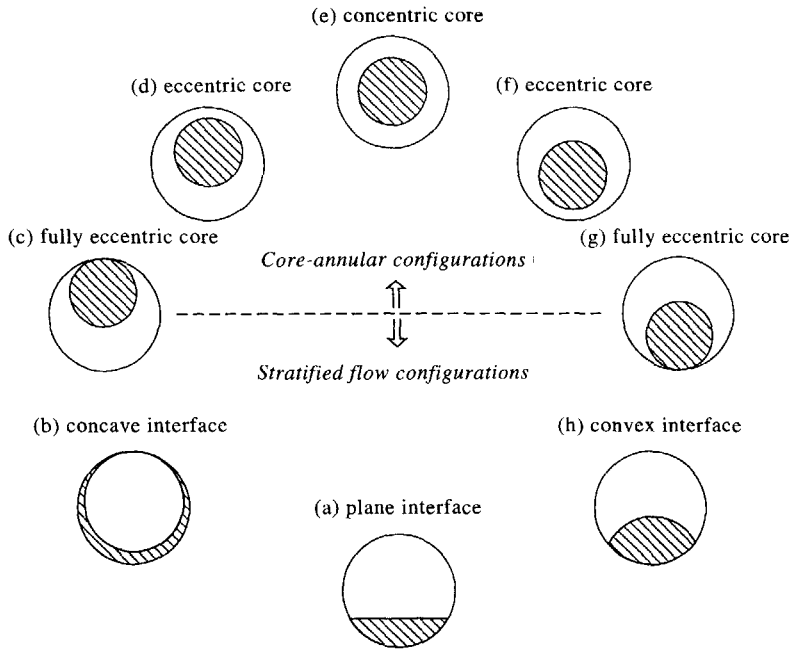

Figure 1. Schematic description of various configurations of stratified flows and core–annular flows.

interfaces, which range between these two extremes of fully eccentric core-annular configurations are typical to systems of $0 < \epsilon_v < 1$, but may also be realized in systems of low Eötvös number due to evolution of hydrodynamic forces which spread one of the fluids over the tube wall. Hydrodynamic forces may also cause the core phase to detach from the wall surface to form an eccentric core–annular configuration (figure 1d, f). When the core eccentricity reduces to zero, the concentric annular flow pattern (figure 1e) is obtained.

Eccentric and concentric core-annular flows were studied extensively, during the sixties and seventies, mainly in conjunction with hydro-transport of solid cylindrical capsules (e.g. Charles 1963; Kruyer *et al.* 1967; Epstein *et al.* 1974; Garner and Raithby 1978) or viscous oil–water systems (e.g. Russell and Charles 1959; Epstein 1963; Bentwich 1970; Ooms 1972; Huang *et al.* 1994). The possible transportation of viscous oils in pipelines, when the oil forms a core phase lubricated by a water annuli, is very attractive—the power requirements are comparable to that for pure-water flow. However, due to density differential (between the oil and water or between the solid capsule and the surrounding fluid) the core phase usually stabilizes in an eccentric position. The core eccentricity affects the system performance (Bentwich *et al.* 1970). Break-up of the top (or bottom) wall film due to the float-up tendency of light (or heavier) core phase results in stratification of the fluids (Hasson *et al.* 1970; Brauner and Moalem Maron 1992b).

The problem of laminar stratified flows with curved interfaces was tackled by Bentwich (1964, 1976) and recently by Brauner *et al.* (1995, 1996). The latter presented a complete analytical solution for laminar stratified flows, whereby the interface curvature is obtained as an integral part of the solution, and is therefore, applicable to a variety of two-fluid systems. The solution shows that the interaction between the stratified layers and the resulting flow characteristics are significantly affected by the configuration of the interface. The relaxation of plane interface assumption in systems of finite ϵ_v results in a large variation of the flow configuration, *in situ* holdup, pressure drop and the associated velocity profiles and shear stress distribution. The largest effects of the interfacial curvature on the two-phase flow characteristics are obtained as the stratified flow configuration approaches either one of the two extremes corresponding to a fully eccentric core.

Thus, the solution of the flow equations for fully eccentric core–annular configuration is of importance for predicting the system performance and flow characteristics under limiting conditions of both and annular and stratified flow patterns and along the transitional boundary between these two patterns. However, the analytical solutions available either for eccentric core flows (Bentwich *et al.* 1970) or stratified flows (Bentwich 1960; Brauner *et al.* 1996, 1995) fail in

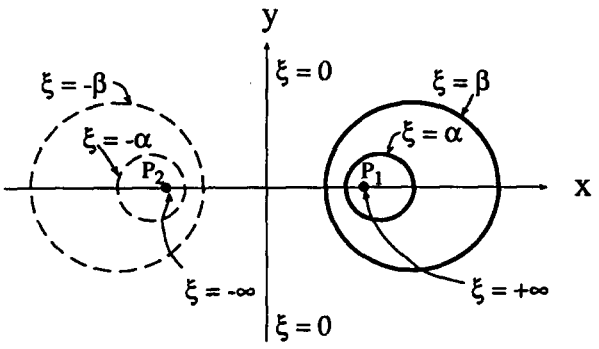

a. Bipolar coordinates; ξ = constant

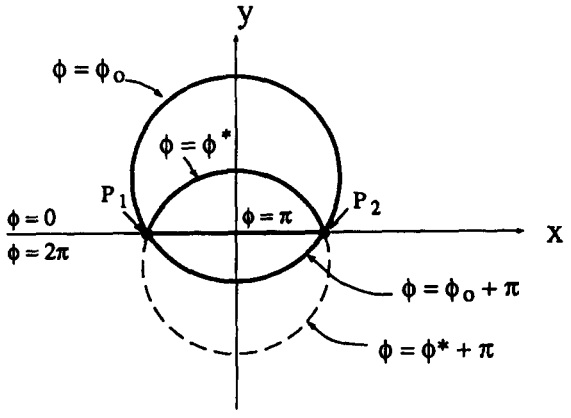

b. Bipolar coordinates; ϕ = constant

Figure 2. Bipolar coordinate system.

the extreme of fully eccentric core–annular configuration. Moreover, close to this limit, although a formal solution exists, the computation becomes tedious (Brauner *et al.* 1995). The source of the difficulties is further elucidated below. Analytical solutions are available only for the case of fully eccentric fixed (rigid) cylinder (Caldwell 1930; Garner and Raithby 1978).

This study is aimed at establishing an analytical solution for laminar *fully* eccentric core–annular flows. This solution further elucidates the range of variation of the two-phase flow characteristics associated with annular and stratified configurations and with the transition between these flow patterns.

2. COORDINATE SYSTEM

2.1. Failure of the bipolar coordinate system

The bipolar coordinate system has been used extensively to solve single phase and two phase systems (e.g. Happel and Brenner 1965). Here however, a brief note is made to point out its limitations in describing the fully eccentric core–annular configuration. This is illustrated by presenting the bipolar coordinates for annular and stratified configurations (figure 2(a) and (b), respectively).

Figure 2(a) corresponds to an eccentric core–annular flow configurations, whereby the tube wall is represented by $\xi = \beta$ while the two-fluid interface coincide with $\xi = \alpha$. Hence, the eccentric

core–annular configuration in the x–y domain maps into a semi infinite strip in the (ϕ, ξ) domain defined by:

$$\text{Annular phase:} \quad \beta < \xi \leqslant \alpha$$
$$0 \leqslant \phi \leqslant 2\pi \qquad [2.1]$$
$$\text{Core phase:} \quad \alpha < \xi < \infty$$
$$0 \leqslant \phi \leqslant 2\pi \qquad [2.2]$$

where:

$$\alpha = \cos h^{-1}\left[\frac{(R + R_c) - E^2(R - R_c)}{2ER_c}\right] \qquad [2.3]$$

$$\beta = \cos h^{-1}\left[\frac{(R + R_c) + E^2(R - R_c)}{2ER}\right] \qquad [2.4]$$

$$E = \frac{e}{R - R_c}. \qquad [2.5]$$

Here R, R_c are the tube and core radius, respectively, and e is the (dimensional) core eccentricity.

For stratified two-phase flows with curved interfaces, the flow domains are confined by curves of ϕ = constant, as in figure 2(b). The pipe perimeter and the interface between the fluids are isolines of coordinates ϕ, so that the upper section of the tube wall which bounds the lighter phase is represented by ϕ_0, while the bottom of the tube, which bounds the heavier phase is represented by $\phi = \phi_0 + \pi$. The interface extends from P_1 to P_2. Thus, the triple points (TP), where the two-fluids interface meets the solid wall are at the two poles of the bipolar system. The interface coincide with the curve of $\phi = \phi^*$, convex interface for $\phi^* < \pi$ and concave interface for $\phi^* > \pi$. In particular, $\phi^* = \pi$ corresponds to the case of plane interface. Thus, the two-phase domains map into two infinite strips in the (ϕ, ξ) domain and are defined by:

$$\text{Upper phase:} \quad -\infty < \xi < \infty$$
$$\phi_0 < \phi < \phi^* \qquad [3.1]$$
$$\text{Lower phase:} \quad -\infty < \xi < \infty$$
$$\phi^* < \phi < \phi_0 + \pi. \qquad [3.2]$$

If the bipolar system is used for the fully eccentric core–annular configuration, then $\phi_0 = 0$, $\phi^* = 0$ or $\phi_0 = \pi$, $\phi^* = 2\pi$. The case of $(\phi_0, \phi^* = 0)$ corresponds to a lower heavier phase which forms the core phase in contact with the tube bottom. The other case of $\phi_0 = \pi$, $\phi^* = 2\pi$ describes a fully eccentric core of the upper lighter phase, touching the upper tube wall. In both cases, the two-poles of the coordinate system merge into a single pole at the system (single) triple point.

When ϕ_0, $\phi^* = 0$, the entire flow domain of annular upper phase in the bipolar coordinate degenerates to a line, $\phi = 0$; for instance, it is no longer possible to distinguish between points located on the meridian, along $\xi = 0$ from the upper wall to the fluids interface. Similarly, when $\phi_0 = \pi$ and $\phi^* = 2\pi$ the flow domain of the lower annular phase degenerates into the line $\phi = 2\pi$.

The same problem arises when the bipolar system is applied for eccentric annular configuration (figure 2a). For a fully eccentric core, $E = 1$ in [2], whereby both α and β reduce to zero. Therefore, here too, the flow domain of the annular phase degenerates into a line, $\xi = 0$. Thus, the bipolar system fails to describe the flow field for fully eccentric core–annular configuration.

2.2. The unipolar coordinate system

The natural coordinate system to handle the geometry of a fully eccentric core is depicted in figure 3. Curves of constant r_1 represent a system of fully eccentric circles of radius r_1 and centered at $(0, r_1)$. In particular, $r_1 = R_c$ represents the two fluids interface and $r_1 = R$ coincides with the tube inner surface. Curves of r_2 = constant represent a second system of fully eccentric circles, which are orthogonal to curves of constant r_1, with radius r_2 and a center at $(r_2, 0)$. Thus, both systems

of circles are tangent to the origin. The value of $r_2 \to \infty$ corresponds to the y-axis. The (r_1, r_2) coordinate system is actually a degenerated bipolar coordinate system, where the two poles merge into a single pole at the TP point ($x = 0, y = 0$), yielding a unipolar coordinate system.

A more convenient coordinate system for solving the Laplace equation is obtained by considering the transformation which evolve from the reciprocal of r_1, r_2 and is associated with equal Lamé coefficients:

$$H_{\rho_1} = H_{\rho_2} = \left[\left(\frac{\partial x}{\partial \rho_1}\right)^2 + \left(\frac{\partial y}{\partial \rho_1}\right)^2\right]^{1/2} = \frac{2}{\rho_1^2 + \rho_2^2} \qquad [4.1]$$

$$\rho_1 = \frac{1}{r_1} = \frac{2y}{x^2 + y^2}; \quad \rho_2 = \frac{1}{r_2} = \frac{2x}{x^2 + y^2} \qquad [4.2]$$

or:

$$x = \frac{2\rho_2}{\rho_1^2 + \rho_2^2}; \quad y = \frac{2\rho_1}{\rho_1^2 + \rho_2^2}. \qquad [4.3]$$

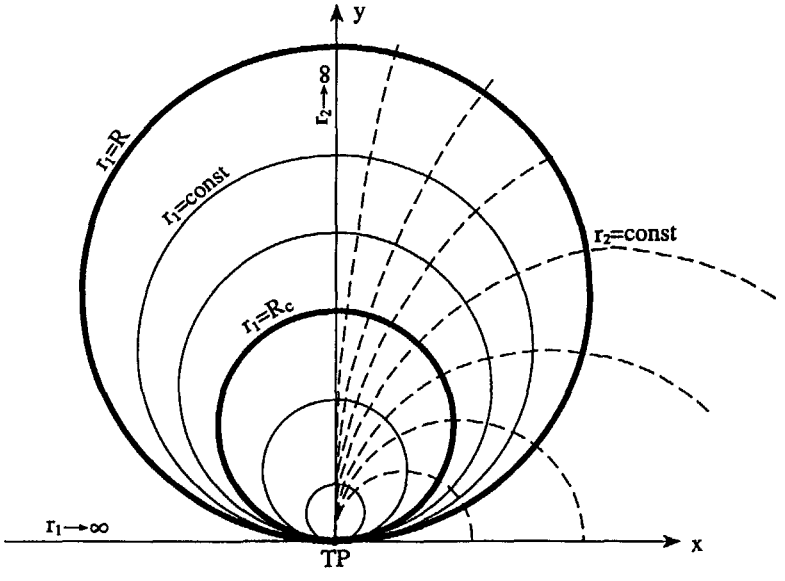

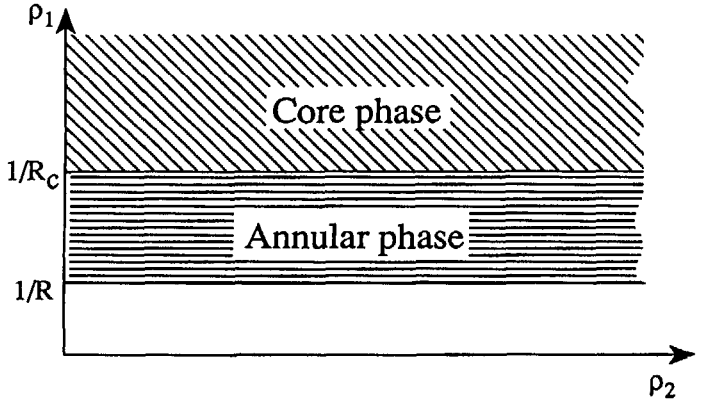

Figure 3. Unipolar coordinate system.

The (ρ_1, ρ_2) coordinate system is similar to 'tangent circles' coordinates, presented in Moon and Spencer (1988).

Figure 3 shows that half of the physical domain of a fully eccentric core–annulus geometry (which is symmetric with respect to $\rho_2 = 0$) maps into a semi infinite domain in the (ρ_1, ρ_2) coordinates, where the two-phases domains are defined by:

$$\text{Annular (upper) phase:} \quad 1/R < \rho_1 < 1/R_c; \; x \geqslant 0$$
$$0 < \rho_2 < \infty \qquad [5.1]$$
$$\text{Core (lower) phase:} \quad 1/R_c < \rho_1 < \infty; \; x \geqslant 0$$
$$0 < \rho_2 < \infty. \qquad [5.2]$$

3. THE FLOW EQUATIONS

Consider the laminar flow of two immiscible fluids in a fully eccentric core configuration (figure 3). For steady and fully developed flow, the Stokes equations for the two-phases in the unipolar coordinate system (ρ_1, ρ_2) are:

$$\frac{(\rho_1^2 + \rho_2^2)^2}{4}\left[\frac{\partial^2 V_1}{\partial \rho_1^2} + \frac{\partial^2 V_1}{\partial \rho_2^2}\right] = -\frac{1}{\mu_1}\frac{\partial p}{\partial z} \qquad [6.1]$$

$$\frac{(\rho_1^2 + \rho_2^2)^2}{4}\left[\frac{\partial_2 V_2}{\partial \rho_1^2} + \frac{\partial^2 V_2}{\partial \rho_2^2}\right] = -\frac{1}{\mu_2}\frac{\partial p}{\partial z} \qquad [6.2]$$

where V_1, V_2 are the phases velocities in the axial direction, μ_1, μ_2 are the fluids dynamic viscosities and $\partial p/\partial z$ is the pressure gradient in the axial direction.

The boundary conditions which are to be satisfied are:

(a) No-slip at the tube wall:

$$(V_1)_{\rho_1 = 1/R} = 0 \qquad [7.1]$$

$$(V_1)_{\rho_2 = \infty} = 0; \quad (V_2)_{\rho_2 = \infty} = 0; \qquad [7.2]$$

$$(V_2)_{\rho_1 = \infty} = 0. \qquad [7.3]$$

Note that boundary condition [7.2] relates to the triple point TP, where the phases interface touches the tube wall. This additional condition evolves due to the transformation from the physical finite flow domain to the mathematically infinite domain in the (ρ_1, ρ_2) coordinate system.

(b) Continuity of velocities and shear stresses across the free interface, at $\rho_1 = \rho_c = 1/R_c$:

$$(V_1)_{\rho_1 = \rho_c} = (V_2)_{\rho_1 = \rho_c} \qquad [7.4]$$

$$\left(\mu_1 \frac{\partial V_1}{\partial \rho_2}\right)_{\rho_1 = \rho_c} = \left(\mu_2 \frac{\partial V_2}{\partial \rho_2}\right)_{\rho_1 = \rho_c}. \qquad [7.5]$$

Boundary condition [7.5] is derived based on the orthogonality feature of the coordinate system and considering it is applied along the interface which is an isoline of ρ_1.

It is convenient to use the following non-dimensional form of the flow equations [6] and boundary conditions [7]:

$$\frac{(\xi_1^2 + \xi_2^2)^2}{4}\left[\frac{\partial^2 \tilde{V}_1}{\partial \xi_1^2} + \frac{\partial^2 \tilde{V}_1}{\partial \xi_2^2}\right] = 1 \qquad [8.1]$$

$$\frac{(\xi_1^2 + \xi_2^2)^2}{4}\left[\frac{\partial^2 \tilde{V}_2}{\partial \xi_1^2} + \frac{\partial^2 \tilde{V}_2}{\partial \xi_2^2}\right] = \tilde{\mu} \qquad [8.2]$$

$$(\tilde{V}_1)_{\xi_1 = 1} = 0; \tag{9.1}$$

$$(\tilde{V}_{1,2})_{\xi_2 = \infty} = 0; \tag{9.2}$$

$$(\tilde{V}_2)_{\xi_1 = \infty} = 0; \tag{9.3}$$

$$(\tilde{V}_1)_{\xi_1 = \xi_c} = (\tilde{V}_2)_{\xi_1 = \xi_c}; \tag{9.4}$$

$$\left(\tilde{\mu}\frac{\partial \tilde{V}_1}{\partial \xi_2}\right)_{\xi_1 = \xi_c} = \left(\frac{\partial \tilde{V}_2}{\partial \xi_2}\right)_{\xi_1 = \xi_c} \tag{9.5}$$

where

$$\xi_{1,2} = (\rho_{1,2})R; \quad \xi_c = R/R_c; \quad \tilde{\mu} = \mu_1/\mu_2$$

$$\tilde{V}_{1,2} = V_{1,2}/V_R; \quad V_R = -\frac{R^2}{\mu_1}\frac{\partial p}{\partial z}. \tag{10}$$

The reference velocity, V_R, is a characteristic velocity obtained with the annular (upper) phase flowing alone in the pipe under a pressure drop identical to that developed in the two-phase flow system.

4. VELOCITY PROFILES

The general solution of the non-homogeneous set in [8] is composed of particular solutions $\tilde{V}_{1p}$, $\tilde{V}_{2p}$ and homogeneous solutions $\tilde{V}_{1h}$, $\tilde{V}_{2h}$. In view of the non-homogeneous terms in [8], the following particular solutions are taken:

$$\tilde{V}_{1p} = \frac{1}{\xi_1^2 + \xi_2^2}; \quad \tilde{V}_{2p} = \frac{\tilde{\mu}}{\xi_1^2 + \xi_2^2}. \tag{11}$$

The solution of the homogeneous two-dimensional Laplace equations can be obtained in the form of the following Fourier integrals (see appendix A):

$$\tilde{V}_{1h} = \int_0^\infty \Phi_1(\omega, \xi_1)\cos(\omega\xi_2)\,d\omega; \quad 1 \leqslant \xi_1 \leqslant \xi_c \tag{12.1}$$

$$\tilde{V}_{2h} = \int_0^\infty \Phi_2(\omega, \xi_2)\cos(\omega\xi_2)\,d\omega; \quad \xi_c \leqslant \xi_1 \leqslant \infty \tag{12.2}$$

where $\Phi_1(\omega, \xi_1)$, $\Phi_2(\omega, \xi_2)$ are the spectral functions [A5.1] and [A5.2].

Combining [12] with the particular solutions [11] yields the general solution for the non-dimensional velocity profiles in the two phases:

$$\tilde{V}_1 = \frac{1}{\xi_1^2 + \xi_2^2} - \frac{1}{\xi_c}(I_1 + I_2) \tag{13.1}$$

$$\tilde{V}_2 = \tilde{\mu}\left[\frac{1}{\xi_1^2 + \xi_2^2} - \frac{1}{\xi_c}I_3\right], \tag{13.2}$$

where:

$$I_1 = \int_0^\infty \left[1 + \frac{(1+\tilde{\mu})(1-\xi_c)}{(1-\tilde{\mu})\,e^{2(1-\xi_c)\omega} - (1+\tilde{\mu})}\right] e^{-\omega\xi_1}\cos(\omega\xi_2)\,d\omega; \quad 1 \leqslant \xi_1 \leqslant \xi_c$$

$$I_2 = \int_0^\infty \left[\frac{(1-\tilde{\mu})(\xi_c-1)\,e^{(\xi_1-2\xi_c)\omega}}{(1-\tilde{\mu})\,e^{2(1-\xi_c)\omega} - (1+\tilde{\mu})}\right]\cos(\omega\xi_2)\,d\omega; \quad 1 \leqslant \xi_1 \leqslant \xi_c$$

$$I_3 = \int_0^\infty \left[1 + \frac{2(1-\xi_c)}{(1-\tilde{\mu})\,e^{2(1-\xi_c)\omega} - (1+\tilde{\mu})}\right] e^{-\omega\xi_1}\cos(\omega\xi_2)\,d\omega; \quad \xi_c \leqslant \xi_1 \leqslant \infty. \qquad [14]$$

5. SHEAR STRESSES

Once the problem is solved for the velocity profiles, the local shear stresses in both phases domains can be derived. Of particular interest is the shear stress distribution over the tube wall and over core interface. These interfaces are isolines of coordinates ξ_1 in the (ξ_1, ξ_2) orthogonal coordinate system; Hence, the wall shear stress is obtained by:

$$\tau_w = \frac{\mu_1}{H_\xi}\left(\frac{\partial V_1}{\partial \xi_1}\right)_{\xi_1 = 1}$$

$$\tilde{\tau}_w = \frac{\tau_w}{\tau_R} = \frac{2}{\xi_2^2+1} + (\xi_2^2+1)\int_0^\infty \omega\cos(\omega\xi_2)e^{-\omega}\left[\xi_c - 2 + \frac{(\xi_c-1)(1+\tilde{\mu})}{(1-\tilde{\mu})\,e^{2\omega(1-\xi_c)} - (1+\tilde{\mu})}\right]d\omega \qquad [15]$$

where

$$\tau_R = \frac{R}{2}\frac{\partial p}{\partial z}; \quad H_\xi = \frac{2R}{\xi_1^2+\xi_2^2}. \qquad [16]$$

The shear stress at the fluids interface is given by:

$$\tau_c = \frac{\mu_1}{H_\xi}\left(\frac{\partial V_1}{\partial \xi_1}\right)_{\xi_1=\xi_c} = \frac{\mu_2}{H_\xi}\left(\frac{\partial V_2}{\partial \xi_1}\right)_{\xi_1=\xi_c}$$

$$\tilde{\tau}_c = \frac{\tau_c}{\tau_R} = \frac{2\xi_c}{\xi_2^2+\xi_c^2} + \frac{\xi_c^2+\xi_2^2}{\xi_c}\int_0^\infty \left[\frac{2(\xi_c-1)}{(1-\tilde{\mu})e^{2\omega(1-\xi_c)} - (1+\tilde{\mu})} - 1\right]\omega\,e^{-(\omega\xi_c)}\cos(\omega\xi_2)\,d\omega. \qquad [17]$$

6. FLOW RATES AND PRESSURE DROP

The volumetric flow rates of the fluids can be obtained by integrating the (dimensional) velocity field V_1, V_2 over the corresponding flow area A_1 and A_2:

$$Q_1 = 2V_R\int_0^\infty d\xi_2\int_1^{\xi_c}\tilde{V}_1(\xi_1,\xi_2)J(\xi_1,\xi_2)\,d\xi_1 = \frac{\pi R^4}{8\mu_1}\frac{\partial p}{\partial z}\tilde{Q}_1(\xi_c,\tilde{\mu}) \qquad [18.1]$$

$$Q_2 = 2V_R\int_0^\infty d\xi_2\int_1^{\xi_c}\tilde{V}_2(\xi_1,\xi_2)J(\xi_1,\xi_2)\,d\xi_1 = \frac{\pi R^4}{8\mu_2}\frac{\partial p}{\partial z}\tilde{Q}_2(\xi_c,\tilde{\mu}) \qquad [18.2]$$

where $J_{(\xi_1,\xi_2)}$ is the Jacobian of the transformation and is given by:

$$J(\xi_1,\xi_2) = \frac{\partial(x,y)}{\partial(\xi_1,\xi_2)} = H_{\xi_1}H_{\xi_2} = \frac{4R^2}{(\xi_1^2+\xi_2^2)^2}. \qquad [19]$$

The non-dimensional functions $\tilde{Q}_1$ and $\tilde{Q}_2$ represent the flow rate enhancement of each of the corresponding fluids; namely, the ratio of the actual volumetric flow rate of the fluid to its rate for single phase laminar flow in the pipe under the two-phase pressure gradient.

The functions $\tilde{Q}_1$, $\tilde{Q}_2$ are obtained by:

$$\tilde{Q}_1(\xi_c, \tilde{\mu}) = \frac{64}{\pi} \int_0^{\infty} d\xi_2 \int_1^{\xi_c} \left[\frac{1}{\xi_1^2 + \xi_2^2} - \frac{1}{\xi_c}(I_1 + I_2) \right] \frac{d\xi_1}{(\xi_1^2 + \xi_2^2)^2} \qquad [20.1]$$

$$\tilde{Q}_2(\xi_c, \tilde{\mu}) = \frac{64}{\pi} \int_0^{\infty} d\xi_2 \int_{\xi_c}^{\infty} \left[\frac{1}{\xi_1^2 + \xi_2^2} - \frac{1}{\xi_c} I_3 \right] \frac{d\xi_1}{(\xi_1^2 + \xi_2^2)^2}. \qquad [20.2]$$

Obviously, the ratio between the actual flow rates of the two fluids is independent of the pressure drop:

$$\tilde{Q} = \frac{Q_1}{Q_2} = \tilde{\mu}^{-1} \frac{\tilde{Q}_1}{\tilde{Q}_2}. \qquad [21]$$

In the case where the fluids viscosities and flow rates prescribed, [21] with [20.1] and [20.2] can be utilized to solve for the core diameter, $R_c = R/\xi_c$ and the corresponding *in situ* holdup of the core fluid, $\tilde{A}_2 = 1/\xi_c^2$. Then, either of [20.1] or [20.2] can be used to calculate the system pressure drop. The non-dimensional pressure drop (normalized with respect to the superficial pressure drop obtained for laminar single phase flow of either one of the fluids) evolves from [18]:

$$\frac{d\tilde{P}_1}{d\tilde{Z}} = \frac{(dp/dz)}{(dp/dz)_{1s}} = \tilde{Q}_1^{-1}(\xi_c, \tilde{\mu}) \qquad [22.1]$$

$$\frac{d\tilde{P}_2}{d\tilde{Z}} = \frac{(dp/dz)}{(dp/dz)_{2s}} = \tilde{Q}_2^{-1}(\xi_c, \tilde{\mu}). \qquad [22.2]$$

Note that the average wall and interfacial shear stresses, which can be obtained by integrating the corresponding expressions for the local shear stresses, [15] and [17], respectively,

$$\bar{\tau}_w = \frac{2}{\pi} \int_0^{\infty} \frac{\tau_R \tilde{\tau}_w}{(1 + \xi_2^2)} d\xi_2 \qquad [23.1]$$

$$\bar{\tau}_c = \frac{2\xi_c}{\pi} \int_0^{\infty} \frac{\tau_R \tilde{\tau}_c}{(\xi_c^2 + \xi_2^2)} d\xi_2, \qquad [23.2]$$

can also be simply derived based on overall momentum balances over the core and annular phases.

These two momentum balances yield:

$$\frac{\bar{\tau}_w}{\tau_{1s}} = \frac{d\tilde{P}_1}{d\tilde{Z}}; \quad \tau_{1s} = \frac{4\mu_1 Q_1}{\pi R^3} \qquad [24.1]$$

$$\frac{\bar{\tau}_c}{\tau_{2s}} = \tilde{A}_2^{1/2} \frac{d\tilde{P}_2}{d\tilde{Z}}; \quad \tau_{2s} = \frac{4\mu_2 Q_2}{\pi R^3} \qquad [24.2]$$

where τ_{1s}, τ_{2s} are the superficial wall shear stresses obtained with single phase flow of the annular and core phase, respectively.

7. RESULTS AND DISCUSSION

The solution of two-phase laminar flow in a fully eccentric core annular configuration is determined in terms of two parameters; the viscosity ratio of the two fluids, and the flow rates ratio $\tilde{Q} = Q_1/Q_2$. Given these two parameters, all the local and integral flow characteristics associated with a fully-eccentric core configuration can be obtained. Note that $\tilde{\mu} < 1$ corresponds to a viscous core flow lubricated by a less viscous fluid flowing in the annulus, which is of practical interest as a possible way for pressure drop and power reduction in the transportation of viscous oils. The

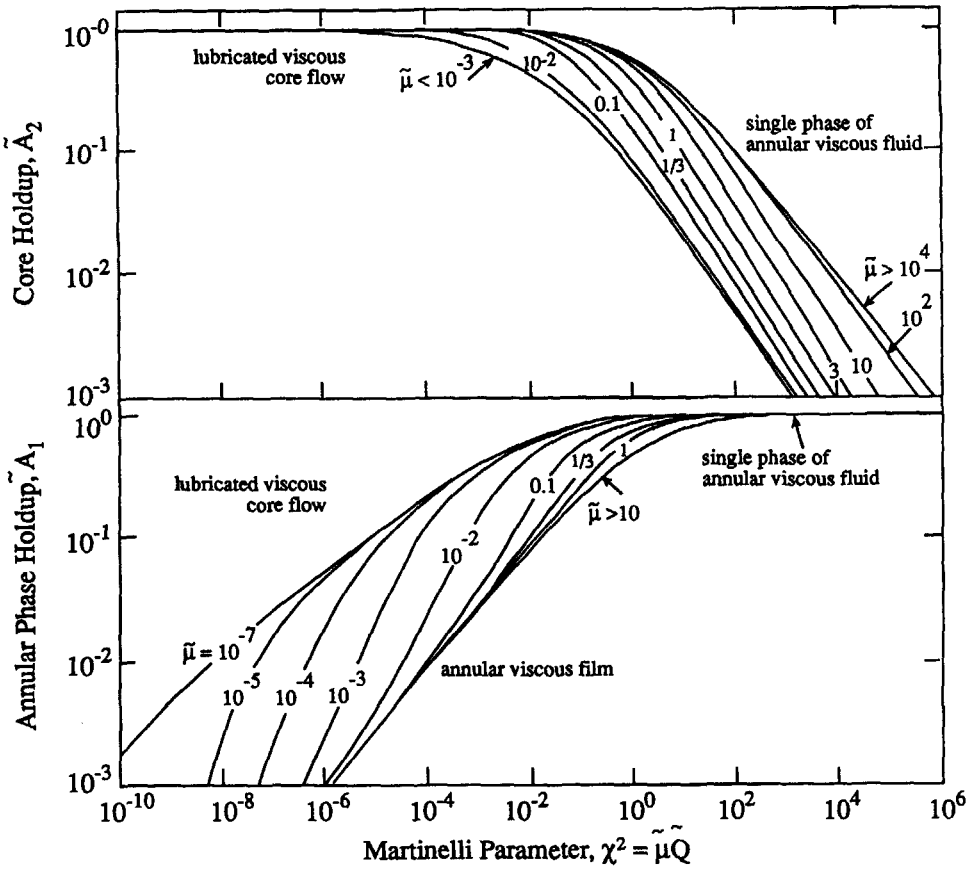

Figure 4. *In situ* holdup in fully eccentric core flows—effect of fluids flow rates and viscosities.

opposite situation of $\tilde{\mu} > 1$, corresponds to a flow of the less viscous fluid in the core as in gas–liquid annular two phase flows. The case of $\tilde{\mu} > 1$ is also of practical interest in liquid–liquid systems, when the viscous fluid is introduced into the annulus in order to protect the pipe wall from corrosion or scale deposition effects (Hasson and Nir 1969; Hasson *et al.* 1970).

Figure 4(a), (b) show the holdup of the core fluid ($\tilde{A}_2$) and annular fluid ($\tilde{A}_1$) for a wide range of fluids viscosity ratio as a function of the Martinelli parameter. Note that $\tilde{\mu}\tilde{Q}$ is the Martinelli parameter for laminar two-phase flows since:

$$\chi^2 = \frac{(dp/dz)_{1s}}{(dp/dz)_{2s}} = \frac{\mu_1}{\mu_2}\frac{Q_1}{Q_2} \qquad [25]$$

Following the trends of the annular phase holdup $\tilde{A}_1$, indicates that for relatively high viscous annular phase, $\tilde{\mu} > 10$, a single parameter $\tilde{\mu}\tilde{Q}$ is practically sufficient to represent the distribution of the two-phases. The region of $\tilde{A}_1 \to 1$ represents practically single flow of the viscous phase with an eccentric thin core of the less viscous phase. This region of $\tilde{A}_1 \to 1$ is preferably demonstrated by the complementary holdup of the core phase, $\tilde{A}_2$, as in figure 4(b), where the continuous thinning of the core with increasing $\tilde{\mu}\tilde{Q}$ can be followed.

By reducing the viscosity ratio, the curve of $\tilde{\mu}_1 = 1$ corresponds to two immiscible fluids of identical viscosities which in laminar two-phase flow yields the same characteristics as those obtained in single phase pipe flow (the density ratio has no effect). For $\tilde{\mu} < 1$, the region of practical interest is that of $\tilde{A}_1 \ll 1$, which corresponds to lubricated viscous core flow. As is indicated in figure 4(a), this region cannot be represented solely by the Martinelli parameter, in which case the core hold-up is a function of both ($\tilde{\mu}\tilde{Q}$) and ($\tilde{\mu}$.)

The system pressure drop is shown in figure 5(a) and (b) for the cases of $\tilde{\mu} > 1$ and $\tilde{\mu} < 1$, respectively. Note that in both cases the system pressure drop is normalized with respect to the superficial pressure drop of the more viscous phase. Thus, both $d\tilde{P}_1/d\tilde{Z}$ and $d\tilde{P}_2/d\tilde{Z}$ represent in

these figures the factor of pressure drop reduction associated with introducing a second less viscous phase. When the annular phase is the more viscous one (figure 5a), the normalized pressure drop is practically a function of the Martinelli parameter only. For this case, where the less viscous phase is not in direct contact with the tube wall, there is no potential for pressure drop reduction as $d\tilde{P}_1/dZ$ does not undershoot the value of 1.0 (except for $\tilde{\mu}\tilde{Q} \sim 2$, where $d\tilde{P}_1/dZ \approx 0.95$).

The other physical situation of lubricated core flow is demonstrated in figure 5(b). Given a flow rate of the viscous phase, Q_2 and $\tilde{\mu}$, the introduction of a small amount of the less viscous phase (low Q_1/Q_2) affects initially a decrease of the two-phase pressure drop. However, eventually, increasing the flow rate of the lubricating phase yields an increase of the pressure drop, where the pressure drop factor exceeds the value of 1.0. As shown in this figure (and also noted with reference to figure 4b), the region of lubricated core flow requires two parameters ($\tilde{\mu}$ and $\tilde{Q}$) to determine the system performance. The zone of single parameter in figure 5(b) corresponds to a high Martinelli parameter, $\tilde{\mu}\tilde{Q} \gg 1$. In this zone, the holdup of the viscous core is less than 5% and $d\tilde{P}_2/dZ \simeq \tilde{\mu}\tilde{Q}$. It practically corresponds to single phase flow of the less viscous phase, where $d\tilde{P}_1/dZ \approx 1$ and is therefore of limited interest. The lubrication zone is bounded by a threshold Martinelli parameter $[\tilde{\mu}\tilde{Q}]_{d\tilde{P}_2/dZ=1} = 0.64$ for $\tilde{\mu} < 10^{-2}$. Hence, the lubrication region is scaled with $\tilde{\mu}$; given the flow rate of the viscous phase, Q_2, the range of flow rates of the less viscous phase which yields a lubricating effect increases with increasing the oil viscosity.

The lubrication zone is, however, better described by plotting the pressure drop factor vs the flow rate ratio. Figure 6(a) shows that the potentials for pressure drop reduction and for power saving both increase with increasing the core viscosity. These are bounded by a minimal value of $\tilde{P}_2 \to 0.025$ approached for $\tilde{\mu} \to 0$. However, the range of flow rates where the maximum lubrication effect is achieved becomes broader as the core viscosity increases. Figure 6 shows that practically, the optimal operational conditions are independent of the fluids viscosity ratio and corresponds to $Q_1/Q_2 \approx 0.1$ ($\approx 10\%$ of the lubricating phase).

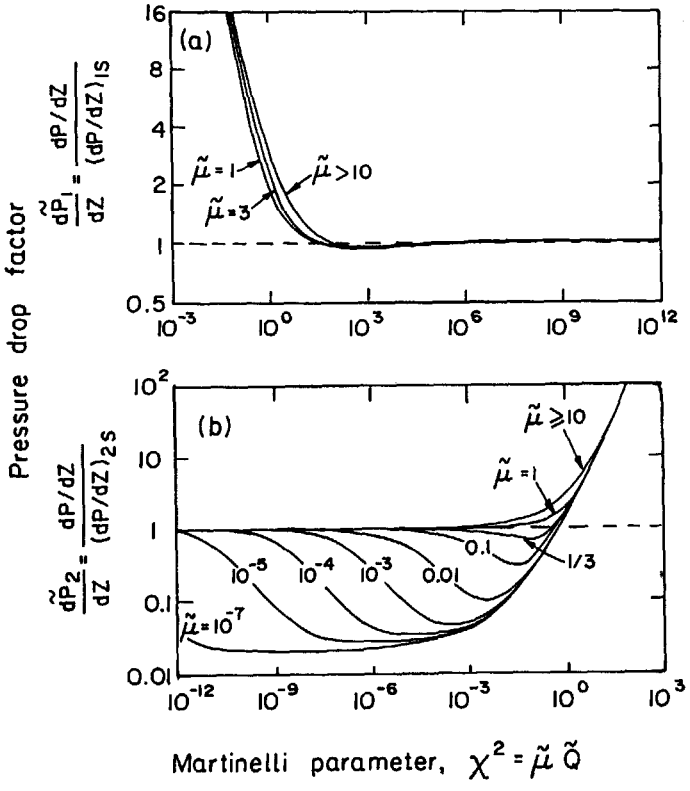

Figure 5. Pressure drop in fully eccentric core flows—effect of fluids flow rates and viscosities.

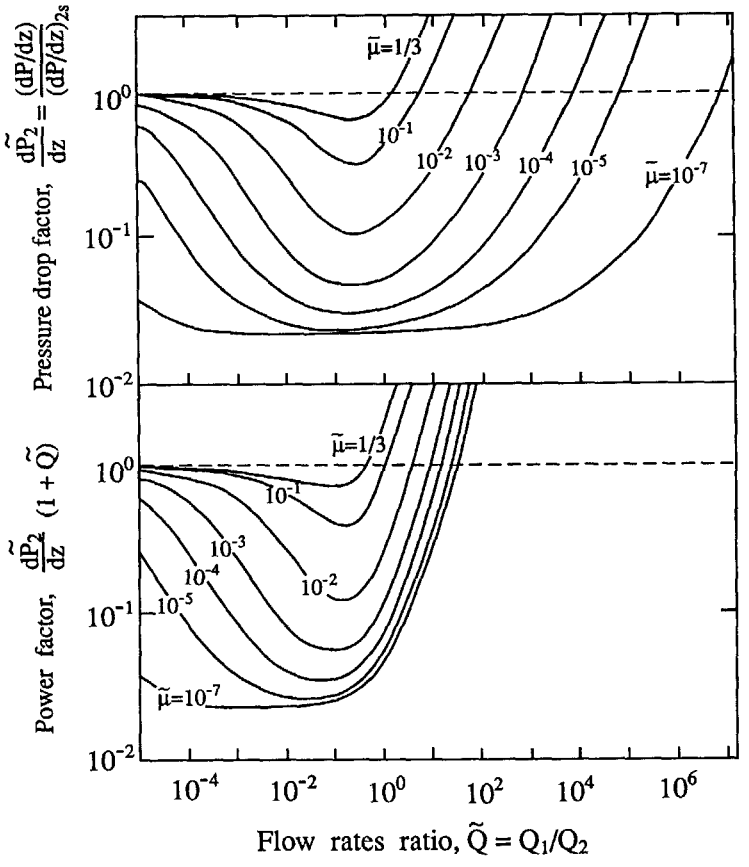

Figure 6. Pressure drop and power reduction in fully eccentric core flows.

8. COMPARISONS WITH CONCENTRIC CORE AND OTHER TWO-PHASE MODELS

Concentric and fully eccentric annular flows represent two extremes which are of practical interest with regard to the performance of core flows. These two extremes are compared here in order to set the bounds for the basic characteristics of *in situ* holdup and pressure drop reduction in core flows. For the sake of completeness, the equations describing the performance of concentric annular flow (e.g. Russell and Charles 1959) are given here in terms of the non-dimensional variables used in this study:

$$a = \frac{1}{\tilde{\mu}}\left[-1 + \left(1 + \frac{\tilde{\mu}}{J@D\tilde{Q}}\right)^{1/2}\right]; \quad a = \frac{\tilde{A}_2}{1 - \tilde{A}_2} \qquad [26.1]$$

$$\frac{d\tilde{P}_2}{d\tilde{Z}} = \frac{1}{\tilde{A}_2^2\left[1 + \frac{2}{\tilde{\mu}}(\tilde{A}_2^{-1} - 1)\right]}. \qquad [26.2]$$

For highly viscous concentric core, $\tilde{\mu} \ll 1$ [26] yields:

$$\tilde{A}_2 = \frac{1}{2\tilde{Q} + 1}; \quad \frac{d\tilde{P}_2}{d\tilde{Z}} = \frac{\tilde{\mu}(2\tilde{Q} + 1)^2}{4\tilde{Q}}. \qquad [27]$$

Note that for a concentric configuration, the average velocity of the annular phase is always smaller than the average velocity of the core phase, independently of the fluids viscosity ratio and flow rates ($\bar{V}_1/\bar{V}_2 = aQ_1/Q_2 < 1$). This ratio, V_1/V_2, is bounded by the value of 1/2, which is approached for large $\tilde{Q}$ as $\tilde{\mu} \to 0$. This is not the case with eccentric core flows. Figure 7 shows that when the core is at a fully eccentric position, the core phase is slowed down. Consequently, the annular phase

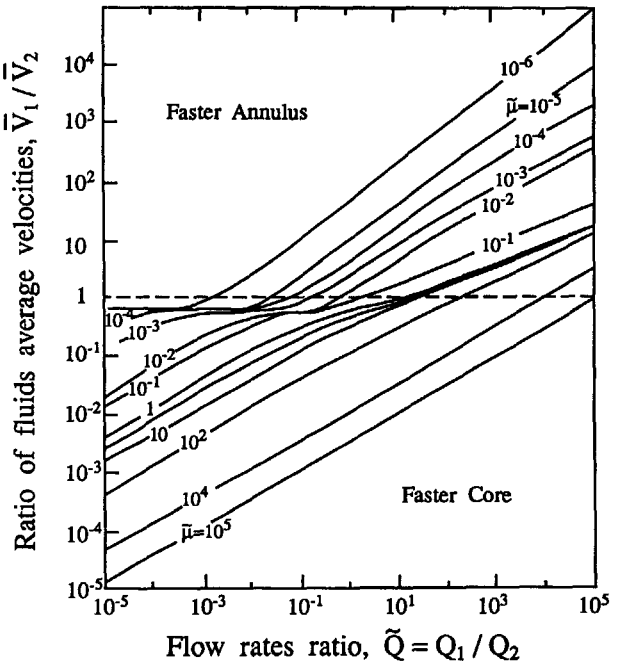

Figure 7. Ratio of the phases average velocities in fully eccentric core flows.

velocity may exceed the core velocity, and for $\tilde{\mu} \ll 1$ the annular phase is the faster one (except for $\tilde{Q} \ll 1$).

Figures 8 and 9 demonstrate the effect of eccentricity on the performance of core flow systems with either $\tilde{\mu} > 1$ or $\tilde{\mu} < 1$. In viscous core flow, the pressure drop in the concentric configuration,

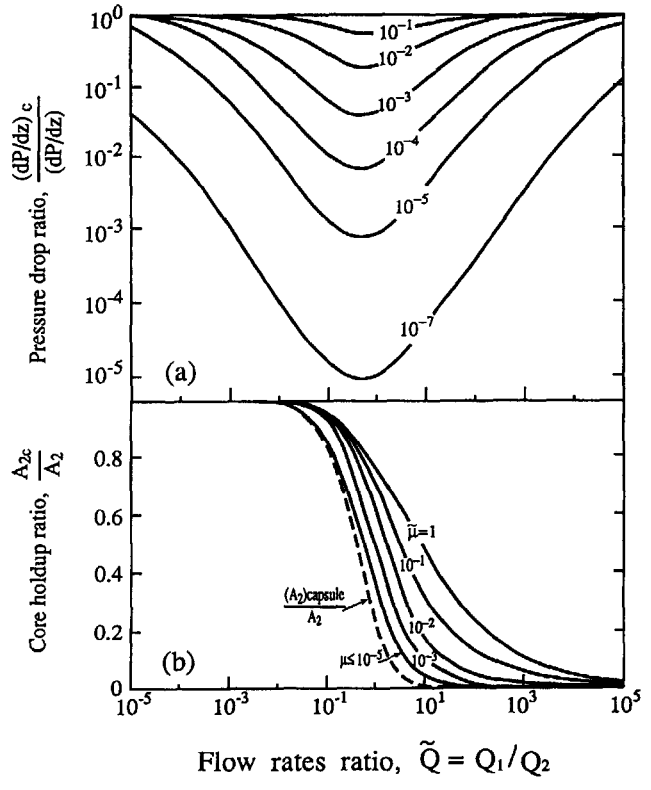

Figure 8. Effect of core eccentricity on the pressure drop and holdup in viscous core flow, $\tilde{\mu} < 1$.

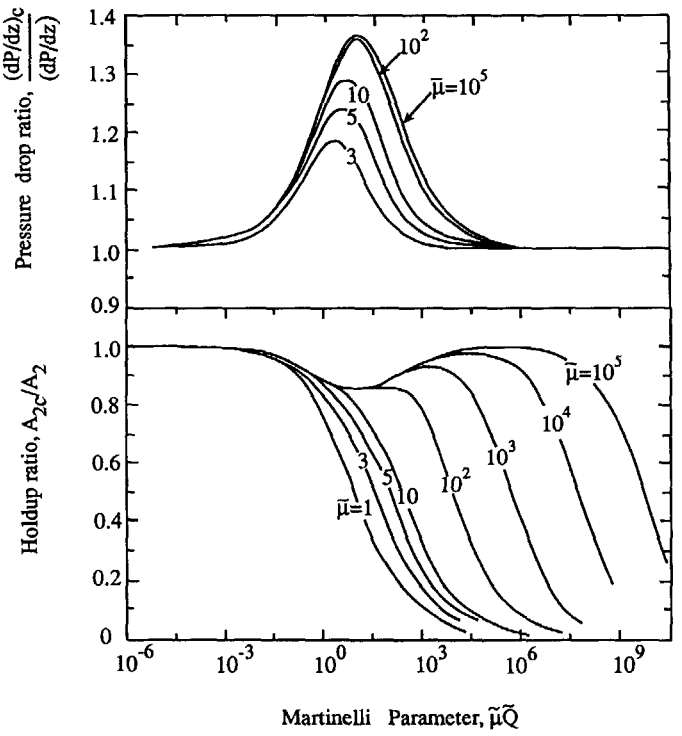

Figure 9. Effect of core eccentricity on the pressure drop and holdup, $\tilde{\mu} > 1$.

$(dP/dZ)_c$ is always lower than that of the eccentric configuration (figure 8a). Note that the pressure drop ratio is also the ratio of the pressure drop reduction factors that can be achieved in these two extremes. For highly viscous concentric core, the lubrication region is wider, $0 < \tilde{\mu}\tilde{Q} < 1$ (compared to $0 < \tilde{\mu}\tilde{Q} < 0.64$ for fully eccentric core). In concentric core flows, the pressure reduction factor is proportional to $\tilde{\mu}$, while with a fully eccentric core, the pressure drop reduction factor is bounded, as shown in figure 6. Therefore, the pressure drop ratio in figure 8(a) decreases with increasing the core viscosity ($\tilde{\mu} \ll 1$). Figure 8(b) shows that the viscous core holdup in concentric core flows, A_{2c} represents a lower bound for that obtained for the core in an eccentric position. This is expected since the proximity of the tube wall slows down the viscous core and a higher flow area is needed to transfer the input flow rate. Note that the decline of the core holdup ratio to zero corresponds to high flow rates ratios, beyond the operational conditions which are of interest for viscous core lubrication. In the lubrication region, the effect of the core eccentricity on the holdup is moderate.

Another reference system which can be used to scale the core holdup in the limit of $\tilde{\mu} \to 0$ (highly viscous core) is the Couette flow of a fully eccentric cylindrical capsule (Epstein *et al.* 1973); In the Couette flow model, the fluid in the annulus is dragged by an eccentric capsule which is moving at a constant velocity, V_c, with zero axial pressure gradient. In the limit of a fully eccentric capsule, the solution of Epstein *et al.* (1973) yields:

$$\tilde{A}_2 = \frac{1}{(1+\tilde{Q})^2}. \qquad [28]$$

There is a basic difference between this capsule model and the present core flow model in the limit of $\tilde{\mu} \to 0$. The rigid capsule is sliding over the tube wall at the capsule velocity, thus the no-slip boundary condition [9.3] at the capsule/wall contact point is not satisfied by the fully eccentric capsule model.

The dashed curve on figure 8(b) represents the ratio of the capsule cross section [28] to the holdup of a fully eccentric core in the limit of $\tilde{\mu} \to 0$. The impact of the no-slip boundary condition on slowing down the highly viscous core phase is reflected by this curve, as the holdup ratio of these two models is always smaller than 1.

Figure 9 shows that for the opposite case of $\tilde{\mu} > 1$, where the viscous liquid forms the annular phase, the core phase holdup is still the lowest at concentric configuration, but the system pressure drop is higher than that obtained for fully eccentric configuration. The effect of the core eccentricity on the pressure drop is most pronounced around $\chi^2 = \tilde{\mu}\tilde{Q} = 10$, but is limited to about 35% for $\tilde{\mu} \ll 1$. This extent of pressure drop increase is due to the reduction of the core phase holdup ($\approx 14\%$ reduction for $\chi^2 \simeq 10$, figure 9b), which for $\tilde{\mu} \gg 1$ is equivalent to the effect of reducing the tube size in single phase Poisuille flow (see appendix B, case b).

The effects of the core eccentricity on the optimal operational conditions in lubricated core flows ($\tilde{\mu} < 1$) are summarized in figures 10 and 11. As noted above, the potentials for pressure drop reduction and power saving in concentric core flows increases with increasing the core viscosity. The phases flow rates ratio, which yields the maximum values of pressure drop and power reduction (figures 10a, 11a) are shown in figures 10(b) and 11(b), respectively. For concentric core, the optimal flow rates ratio increases monotonously with the core viscosity and approaches the value of $\tilde{Q} = 0.5$ for $\tilde{\mu} \to 0$. In this limit of rigid core, the core phase occupies half of the tube cross section, figure 10(c). Maximum power saving is achieved with $\tilde{Q} = 0.3$, where $\tilde{A}_2 = 0.62$. With fully eccentric core, the maximum pressure reduction and power saving get saturated for $\tilde{\mu} \to 0$ at a level of 0.025. But these optimal conditions are achieved with lower amounts of lubricating phase: $\tilde{Q} \to 0$ and $\tilde{A}_2 \to 1$ as $\tilde{\mu} \to 0$. From the practical point of view, however, a certain amount of lubricating phase must

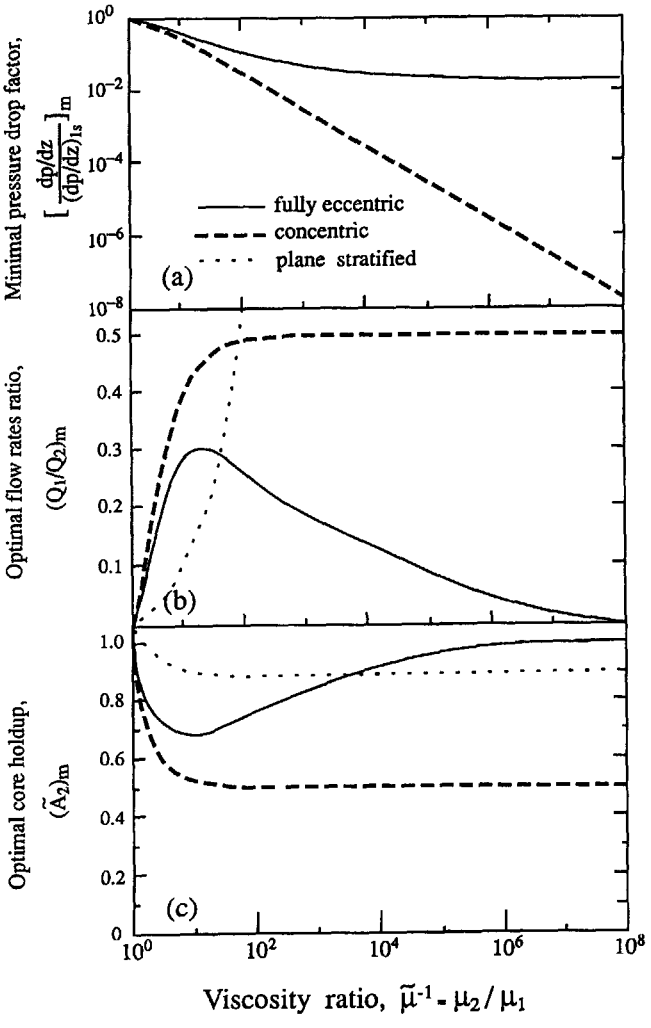

Figure 10. Maximum pressure reduction—effect of fluids viscosities on the optimal operational conditions in stratified flow, concentric and fully eccentric core flows.

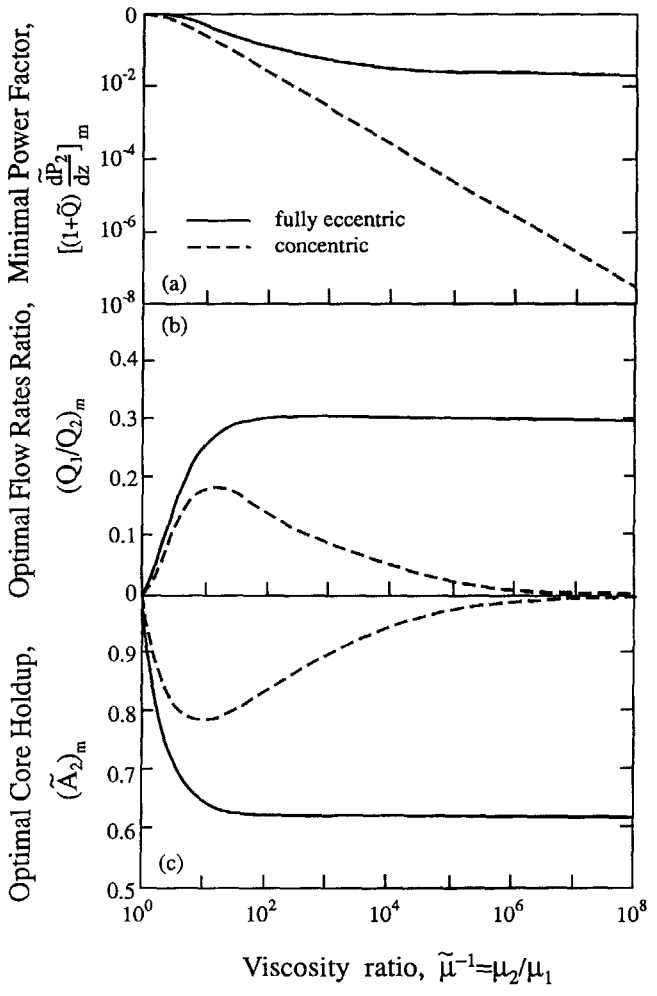

Figure 11. Maximum power reduction—effect of fluids viscosities on the optimal operational conditions in concentric and fully eccentric core flows.

always be added. In view of figure 6, these optimal operational conditions are as well reached with $\tilde{Q} \simeq 0.1$.

It is of interest to note that at this extreme of $\tilde{\mu} \to 0$, the characteristics of fully eccentric core flow resemble those obtained with stratified flow between two infinite plates; In this simple geometry too, the optimal flow rate of the lubricating phase and its holdup approach zero in the limit of highly viscous lubricated phase (Brauner *et al.* 1996a). The minimal pressure drop factor that can be achieved in the two plates geometry is, however, limited to 0.25, 10 times higher than that achieved in a fully eccentric lubricated core flows (75% pressure reduction in plates geometry compared to 97.5% reduction in a configuration of a fully eccentric core).

When the core phase adheres to the tube walls, the core flow configuration may be destroyed and stratification takes place with either curved or plane interface (see figure 1). Analytical solutions for laminar stratified flows with plane, concave or convex interfaces have been recently presented by Brauner *et al.* (1995, 1996a). As the contact area between the viscous phase and the tube wall increases, the potential for pressure drop reduction by adding a lubricating phase is obviously reduced. For comparison, in stratified flow with a plane interface the maximal achievable pressure drop reduction is only about 30% (the minimal value of pressure drop factor is 0.71). This value is approached when the viscosities of the two layers differ by more than two orders of magnitude. For such a high viscosity gap, the Martinelli parameter for which the maximum pressure reduction is achieved and the corresponding layer thicknesses are both independent of the fluid viscosity ratio: $\chi^2 = \tilde{\mu}\tilde{Q} \simeq 0.007$, $\tilde{A}_1 = 0.106$ (the layer thickness of the lubricating fluid is $h/D = 0.19$, Brauner *et*

al. 1996a). Therefore, in the stratified configuration, in order to achieve the maximum reduction of pressure drop, higher oil viscosity (lower $\bar{\mu}$) requires higher Q_1/Q_2, hence higher flow rates of the lubricating phase (dotted curve in figure 10b).

When the interface of the lubricating phase attains a convex shape (figure 1h), the contact area between the viscous phase and the tube wall further increases, and the potential for pressure drop reduction further diminishes. Eventually, when the lubricating phase forms a core at a fully eccentric position (figure 1g) the pressure reduction is limited to a few percents (as noted with reference to figure 5a), which is of no practical value.

9. IMPLICATIONS TO SOLUTIONS OF STRATIFIED FLOWS WITH CURVED INTERFACES

The effect of the interface curvature on the stratified flow characteristics has been recently studied by Brauner *et al.* (1995) and Maron *et al.* (1995). Analytical solutions for the 2-D velocity profiles and shear stresses distribution in the two-phases have been obtained in the bipolar coordinate systems in the form of Fourier integrals. The local and integral flow characteristics have been calculated for concave or convex interfaces ranging from nearly fully eccentric core of the lower phase to nearly fully eccentric core of the upper phase (figure 1).

As explained in section 2.1, the bipolar coordinate system fails in the limit of fully eccentric core annular configuration. When this limit is approached, the calculation becomes tedious.

The difficulties can be understood in view of figure 12, where the spectral functions, which are needed for carrying out the Fourier integrals in the *bipolar* coordinate system, are shown for a particular case of $\bar{\mu} = 0.01$. In the bipolar coordinate system, the fully eccentric viscous core–annular configuration is approached when $\phi_0 \to 180°$ and $\phi^* \to 360°$ (see [3.2] and figure 2b). Note that $\phi^* = 180°$ (and any ϕ_0) corresponds to stratified flows with plane interfaces. The widening of the spectrum of the lubricating phase when approaching the fully eccentric core configuration (figure 12b) introduces convergence problems and increases dramatically the computational effort and time. Consequently, the results obtained in this limit may be deficient.

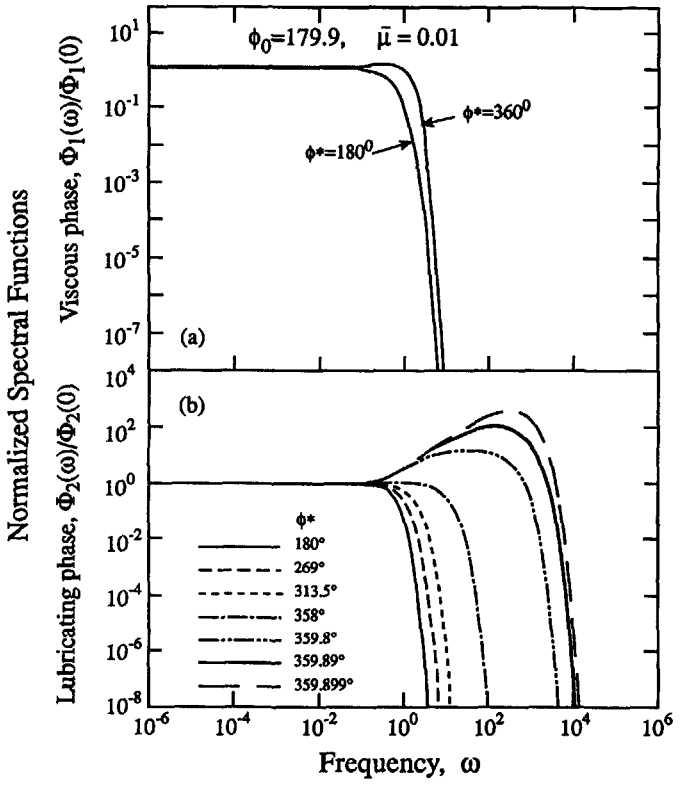

Figure 12. Spectral functions in the bipolar coordinate system, $\bar{\mu} = 0.01$.

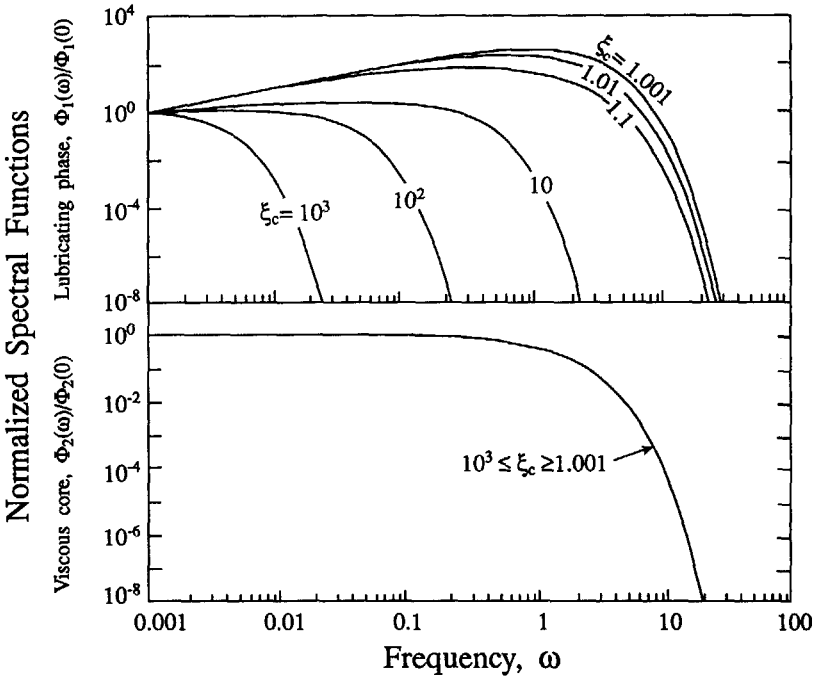

Figure 13. Spectral functions in the unipolar coordinate system, $\tilde{\mu} = 0.01$.

For comparison, the spectral functions for $\tilde{\mu} = 0.01$ and a fully eccentric core configuration, which are obtained in the unipolar coordinate system are shown in figure 13. The narrow spectrums for both phases indicate a clear advantage of the unipolar coordinates in rendering a solvable problem.

Hence, the independent solution obtained in this study for a fully eccentric core–annular configuration is useful also for studying the effect of the *in situ* phases distribution on the flow characteristics, with interface configurations which are encountered in the transition between stratified flow with curved interface and eccentric annular flows.

REFERENCES

Bentwich, M. (1964) Two-phase axial flow in pipe. *Trans. of the ASME, D* **86,** 669–672.

Bentwich, M., Kelly, D. A. I. and Epstein, N. (1970) Two-phase eccentric interface laminar pipeline flow. *J. Basic Eng.* **92,** 32–36.

Bentwich, M. (1976) Two-phase laminar flow in a pipe with naturally curved interface. *Chem. Eng. Sci.* **31,** 71–76.

Brauner, N. (1990) On the relations between two-phase flows under reduced gravity and earth experiments. *Int. Comm. Heat and Mass Transfer* **17,** 271–281.

Brauner, N. and Moalem Maron, D. (1989) Two-phase liquid–liquid stratified flow. *Physico-Chem. Hydrodynam.* **11,** 487–506.

Brauner, N. and Moalem Maron, D. (1992a) Stability analysis of stratified liquid–liquid horizontal flow. *Int. J. Multiphase Flow* **18,** 103–121.

Brauner, N. and Moalem Maron, D. (1992b) Flow pattern transitions in two-phase liquid–liquid horizontal tubes. *Int. J. Multiphase Flow* **18,** 123–140.

Brauner, N., Rovinsky, J. and Moalem Maron, D. (1995) Analytical solution of laminar stratified flow with curved interfaces. *Proceedings of the NURETH-7 Meeting*, ANS, Vol. 1, pp. 192–211.

Brauner, N., Rovinsky, J. and Moalem Maron, D. (1996a) Analytical solution for laminar–laminar two-phase flow in circular conduits, *Chem. Eng. Comm.* **141–142,** 103–143.

Brauner, N., Rovinsky, J. and Moalem Maron, D. (1996b) Determination of the interface curvature in stratified two-phase systems by energy considerations. *Int. J. Multiphase Flow* **22,** 1167–1185.

Caldwell, J. (1930) *J. Roy. Tech. Coll., Glasgow* **2,** 203–220.

Charles, M. E. (1963) The pipeline flow of capsules—Part 2: Theoretical analysis of the concentric flow of cylindrical forms. *Can. J. Chem. Eng.* **41,** 46–51.

Epstein, N. (1963) Concentric laminar flows. *Can. J. Chem. Eng.* **41,** 181.

Epstein, N., Bianchi, R. J., Lee, V. T. Y. and Bentwich, M. (1974) Eccentric laminar Couette flow of long cylindrical capsules. *Can. J. Chem. Eng.* **52,** 210–214.

Garner, R. G. and Raithby, G. D. (1978) Laminar flow between a circular tube and a cylindrical eccentric capsule. *Can. J. Chem. Eng.* **56,** 176–180.

Happel, J. and Brenner, H. (1965) *Low Reynolds Number Hydrodynamics*. Prentice-Hall, New York.

Hasson, D., Mann, U. and Nir, A. (1970) Annular flow of two immiscible liquids: I. Mechanisms. *Can. J. Chem. Eng.* **48,** 514–520.

Huang, A., Christodoulou, C., and Joseph, D. D. (1994) Friction factor and holdup studies for lubricated pipelining—II. Laminar and k-ε models of eccentric core flow. *Int. J. Multiphase Flow* **20,** 481–491.

Kruyer, J., Redberger, P. J. and Ellis, H. S. (1967) The pipeline flow of capsules—Part 9. *J. Fluid Mech.* **30,** 513–531.

Moalem Maron, D., Rovinsky, J. and Brauner, N. (1995) Analytical prediction of the interface curvature and its effects on stratified flow characteristics. *Proc. of the Int. Symp. on Two-phase Flow Modeling and Experimentation*, eds G. P. Celata and R. K. Shah, Vol. 1, pp. 163–170.

Moon, P. and Spencer, D. E. (1988) *Field Theory Handbook*. Springer, Berlin.

Ooms, G. (1972) The hydrodynamic stability of core–annular flow of two ideal liquids. *Appl. Sci. Res.* **26,** 147–158.

Russell, T. W. F. and Charles, M. E. (1959) The effect of the less viscous liquid in the laminar flow of two immiscible liquids. *Can. J. Chem. Eng.* **37,** 18–34.

APPENDIX A

Solution of the Homogeneous Laplace Equations

The particular solutions $\tilde{V}_{1p}$, $\tilde{V}_{2p}$ [11] satisfy boundary conditions [9.2] and [9.3]. Hence the homogeneous set of equations and corresponding boundary conditions, which are to be solved, read:

$$\frac{\partial^2 \tilde{V}_{1h}}{\partial \xi_1^2} + \frac{\partial^2 \tilde{V}_{1h}}{\partial \xi_2^2} = 0 \qquad [A1.1]$$

$$\frac{\partial^2 \tilde{V}_{2h}}{\partial \xi_1^2} + \frac{\partial^2 \tilde{V}_{2h}}{\partial \xi_2^2} = 0 \qquad [A1.2]$$

$$(\tilde{V}_{1h})_{\xi_1 = 1} = -\frac{1}{1 + \xi_2^2}; \qquad [A2.1]$$

$$(\tilde{V}_{1h})_{\xi_2 = \infty} = 0; \quad (\tilde{V}_{2h})_{\xi_2 = \infty} = 0; \qquad [A2.2]$$

$$(\tilde{V}_{2h})_{\xi_1 = \infty} = 0; \qquad [A2.3]$$

$$(\tilde{V}_{1h})_{\xi_1 = \xi_c} = (\tilde{V}_{2h})_{\xi_1 = \xi_c} - \frac{(1 - \tilde{\mu})}{\xi_c^2 + \xi_2^2}; \qquad [A2.4]$$

$$\tilde{\mu}\left(\frac{\partial \tilde{V}_{1h}}{\partial \xi_2}\right)_{\xi_1 = \xi_c} = \left(\frac{\partial \tilde{V}_{2h}}{\partial \xi_2}\right)_{\xi_1 = \xi_c}. \qquad [A2.5]$$

Substituting the Fourier integrals for $\tilde{V}_{1h}$ [12.1] and $\tilde{V}_{2h}$ [12.2] in [A1] and [A2] yields the following relations for the spectral functions:

From [A1.1]:

$$\frac{d^2 \Phi_1}{d\xi_1^2} - \Phi_1 = 0 \qquad [A3.1]$$

From [A1.2]:

$$\frac{d^2\Phi_2}{d\xi_1^2} - \Phi_2 = 0. \qquad [A3.2]$$

From [A2.1]:

$$\Phi_1(\omega, 1) = -e^{-\omega}. \qquad [A4.1]$$

From [A2.3]:

$$\Phi_2(\omega, \infty) = 0. \qquad [A4.2]$$

From [A2.4]:

$$\Phi_2(\omega, \xi_c) - \Phi_1(\omega, \xi_c) = \frac{1-\tilde{\mu}}{\xi_c} e^{-\xi_c\omega}. \qquad [A4.3]$$

From [A2.5]:

$$\tilde{\mu}\left(\frac{\partial\Phi_1}{\partial\xi_1}\right)_{\xi_1=\xi_c} = \left(\frac{\partial\Phi_2}{\partial\xi_1}\right)_{\xi_1=\xi_c}. \qquad [A4.4]$$

Note that boundary condition [A2.2] is met by retaining only the $\cos(\omega\xi_2)$ terms in the Fourier integrals [12], thus satisfying the symmetry of the velocity profiles about the meridian at $\xi_2 = 0$ (the vanishing of the $\tilde{V}_{1h}$, $\tilde{V}_{2h}$ as $\xi_2 \to \infty$ is an underlying requirement for applying [12]).

The spectral functions which solve [A3] with boundary conditions[A4] read:

$$\Phi_1(\omega, \xi_1) = -\frac{1}{\xi_c}\frac{[(1-\tilde{\mu})e^{2(1-\xi_c)\omega} - (1+\tilde{\mu})\xi_c] + (1-\tilde{\mu})(\xi_c - 1)e^{2\omega(\xi_1-\xi_c)}}{(1-\tilde{\mu})e^{2(1-\xi_c)\omega} - (1+\tilde{\mu})} e^{-\omega\xi_1} \qquad [A5.1]$$

$$\Phi_2(\omega, \xi_1) = \frac{\tilde{\mu}}{\xi_c}\frac{[2\xi_c + \tilde{\mu} - 1 - (1-\tilde{\mu})e^{2(1-\xi_c)\omega}]}{[(1-\tilde{\mu})e^{2\omega(1-\xi_c)} - (1+\tilde{\mu})]} e^{-\omega\xi_1}. \qquad [A5.2]$$

APPENDIX B

Convergence to Known Solutions

The solutions [13] and [14], obtained for the velocity profiles in two phases which flow in a fully eccentric core–annulus configuration can be further validated in view of their convergence to single phase Poisuille flow in the limits of $\tilde{\mu} = 1$ and $\tilde{\mu} \to \infty$, and to the solution for flow between fully eccentric cylinders when $\tilde{\mu} \to \infty$.

(a) Equal fluids viscosities, $\tilde{\mu} = 1$. For this case:

$$I_1 = \frac{\xi_c\xi_1}{\xi_1^2 + \xi_2^2}; \quad I_2 = 0; \quad I_3 = \frac{\xi_c\xi_1}{\xi_1^2 + \xi_2^2}. \qquad [B1]$$

Hence:

$$\tilde{V}_1 = \tilde{V}_2 = \frac{1-\xi_1}{\xi_1^2 + \xi_2^2}. \qquad [B2]$$

Utilizing the relation between cylindrical coordinate r and (ξ_1, ξ_2):

$$\left(\frac{r}{R}\right)^2 = \left(\frac{x}{R}\right)^2 + \left(\frac{y}{R} - 1\right)^2 = \frac{4\xi_2^2}{(\xi_1^2 + \xi_2^2)^2} + \left[\frac{2\xi_1}{(\xi_1^2 + \xi_2)^2} - 1\right]^2 \qquad [B3]$$

it follows that:

$$\frac{1-\xi_1}{(\xi_1^2 + \xi_2^2)} = -\frac{1}{4}\left(1 - \frac{r^2}{R^2}\right). \qquad [B4]$$

Thus, for $\tilde{\mu} = 1$ the solution in [13] yields the well-known Poisuille flow in a tube of ratius R:

$$V = \tilde{V}V_R = \frac{R^2}{4\mu}\frac{dp}{dz}\left(1 - \frac{r^2}{R^2}\right). \qquad [B5]$$

(b) Rigid annulus, $\tilde{\mu} \to \infty$. For this case:

$$I_3 = \frac{\xi_1}{\xi_1^2 + \xi_2^2}. \qquad [B6]$$

Hence:

$$V_2 = \tilde{\mu}\frac{1 - \xi_1/\xi_c}{\xi_1^2 + \xi_2^2}. \qquad [B7]$$

For cylindrical coordinates centered at the core center:

$$\left(\frac{r}{R}\right)^2 = \left(\frac{x}{R}\right)^2 + \left(\frac{y}{R} - \frac{1}{\xi_c}\right)^2 \qquad [B8]$$

which yields:

$$\frac{1 - \xi_1/\xi_c}{\xi_1^2 + \xi_2^2} = \frac{1}{4}\left[\left(\frac{r}{R}\right)^2 - \frac{1}{\xi_c^2}\right]. \qquad [B9]$$

When [B9] is substituted in [B7], the velocity profile corresponding to Poisuille flow in a pipe of radius R_c is obtained:

$$V_2 = \tilde{V}_2 V_R = \frac{R_c^2}{4\mu_2}\frac{dp}{dz}\left[1 - \frac{r^2}{R_c^2}\right] \qquad [B10]$$

(c) Rigid core, $\tilde{\mu} = 0$. This case corresponds to a fluid of viscosity μ_1 flowing in a fully eccentric annuli formed between two fully eccentric cylinders. The rigid core velocity (in contact with the stationary tube wall) is obviously zero, $V_2 = 0$. Substituting $\tilde{\mu} = 0$ in [13] and [14] yields:

$$\tilde{V}_1 = \frac{1}{\xi_1^2 + \xi_2^2} - \frac{1}{\xi_c}\int_0^\infty \left[\frac{e^{2\omega(1-\xi_c)} - \xi_c}{e^{2\omega(1-\xi_c)} - 1} e^{-\omega\xi_1 + (\xi_c - 1)\frac{e^{\omega(\xi_1 - 2\xi_c)}}{e^{2\omega(1-\xi_c)} - 1}}\right]\cos(\omega\xi_2)\, d\omega \qquad [B11]$$

which can be further rearranged to yield:

$$\tilde{V}_1 = \frac{1}{\xi_1^2 + \xi_2^2} - \int_0^\infty \left[\frac{e^{-\omega\xi_c}\sin h[\omega(\xi_1 - 1)]}{\xi_c \sin h[\omega(\xi_c - 1)]} + \frac{e^{-\omega}\sinh(\omega(\xi_c - \xi_1))}{\sin h[\omega(\xi_c - 1)]}\right]\cos(\omega\xi_2)\, d\omega. \qquad [B12]$$

The form [B12] is identical to the solution obtained by Garner and Raithby (1978) for the case of fully eccentric capsule (in their notation, $\xi_2 = 2R\psi^*$, $\xi_1 = 2R\eta$, $\omega = n/2R$).

For $R_c \to 0$, $\xi_c \to \infty$, [B12] reduced to:

$$V_1 = \frac{1}{\xi_1^2 + \xi_2^2} - \int_0^\infty e^{-\omega\xi_1}\cos\omega\xi_2\, dw = \frac{1 - \xi_1}{\xi_1^2 + \xi_2^2} \qquad [B13]$$

which is identical to the expression obtained for the velocity profile of single phase Poisuille flow in the (ξ_1, ξ_2) coordinates, [B2].